Engineering 21 (2023) 92–100

Contents lists available at ScienceDirect

Engineering

journal homepage: www.elsevier.com/locate/eng

Research
Green Chemical Engineering—Article

Continuous-Flow Synthesis of the Nucleobase Unit of Remdesivir

Yongxing Guo [a], Minjie Liu [b,c], Meifen Jiang [b,c], Yuan Tao [b,c], Dang Cheng [b,c,*], Fen-Er Chen [a,b,c,*]

[a] Pharmaceutical Research Institute, Key Laboratory of Green Chemical Engineering Process of Ministry of Education, School of Chemical Engineering and Pharmacy, Wuhan Institute of Technology, Wuhan 430205, China
[b] Engineering Center of Catalysis and Synthesis for Chiral Molecules, Department of Chemistry, Fudan University, Shanghai 200433, China
[c] Shanghai Engineering Center of Industrial Asymmetric Catalysis for Chiral Drugs, Shanghai 200433, China

ARTICLE INFO

Article history:
Received 19 February 2021
Revised 20 June 2021
Accepted 6 July 2021
Available online 26 March 2022

Keywords:
Flow chemistry
Continuous multistep synthesis
Microreaction technology
Reaction–separation integration

ABSTRACT

In this work, the nucleobase unit of the antiviral drug remdesivir, 7-bromopyrrolo[2,1-*f*][1,2,4]triazin-4-amine, was synthesized through five-step continuous flow. By adapting batch synthetic chemistry, 7-bromopyrrolo[2,1-*f*][1,2,4]triazin-4-amine was successfully produced through sequential flow operations from the widely available and inexpensive starting material pyrrole. Under optimal flow conditions, 7-bromopyrrolo[2,1-*f*][1,2,4]triazin-4-amine was obtained in 14.1% isolated yield in a total residence time of 79 min with a throughput of 2.96 $g \cdot h^{-1}$. The total residence time was significantly shorter than the total time consumed in batch procedures (> 26.5 h). In flow, the highly exothermic Vilsmeier–Haack and N-amination reactions involving hazardous and unstable intermediates, oxidative liquid–liquid biphasic transformation, and a bromination reaction requiring strict cryogenic conditions are favorably facilitated. The salient feature of this synthesis is that the workup procedures are fully integrated into the reaction sequences by deploying dedicated equipment and separation units, thus forming a streamlined continuous-flow system that maximizes the overall process efficiency. This method represents a greener and more sustainable process to prepare this nucleobase unit with high efficiency and safety.

1. Introduction

Remdesivir has attracted worldwide attention during the devastating public health crisis of coronavirus disease 2019 (COVID-19), caused by severe acute respiratory syndrome coronavirus 2 (SARS-CoV-2). This phosphoramidate nucleotide analog, which is marketed as Veklury [1,2], is still being evaluated alone or in combination with other medications in a host of clinical trials across the globe to treat patients infected with COVID-19 [3], since divergent points of view on its effectiveness exist [1,2,4]. Remdesivir was authorized for emergency use in the United States and Japan and for conditional use in the European Union (EU), Singapore, Australia, Republic of Korea, and Canada during the first wave of the pandemic [1], allowing hospitalized adult and pediatric COVID-19 patients to receive remdesivir treatments. Up to June 2021, COVID-19 has caused approximately 175 million infections and 3.8 million deaths worldwide [5]. Worse still, the number of confirmed cases of COVID-19 is still on the rise globally, with several even more contagious variants raising fresh alarm around the world [6,7]. Given the global scale of the pandemic and the potentially astronomical demand for the active pharmaceutical ingredient (API) required for the production of remdesivir, ensuring a sufficient supply of this compound is likely to be an urgent matter [8]. Although considerable efforts have been put into improving the synthetic approach for remdesivir, the currently used batch production is still a lengthy, resource-intensive process that must be completed sequentially and is considerably hindered by several specialized organic chemistry steps that are difficult to operate at scale and are accompanied by low yields [9]. The complex batch process appears to impact the ability to rapidly produce large quantities of remdesivir in an emergency situation such as the COVID-19 pandemic; furthermore, it leads to high cost and hence limits the broad accessibility of this drug [9]. Therefore, the development of a highly efficient and scalable synthetic protocol to prepare remdesivir is required.

From a retrosynthetic analysis (Fig. 1), remdesivir can be assembled from three different building blocks, including a ribolactone unit **2**, a phosphoramidate unit with a stereogenic phosphorus center **3**, and an adenine-mimicking nucleobase unit **4** (i.e., 7-halogenpyrrolo[2,1-*f*][1,2,4]triazin-4-amine) [10,11]. Because a

* Corresponding authors.
E-mail addresses: dcheng@fudan.edu.cn (D. Cheng), rfchen@fudan.edu.cn (F.-E. Chen).

https://doi.org/10.1016/j.eng.2021.07.029

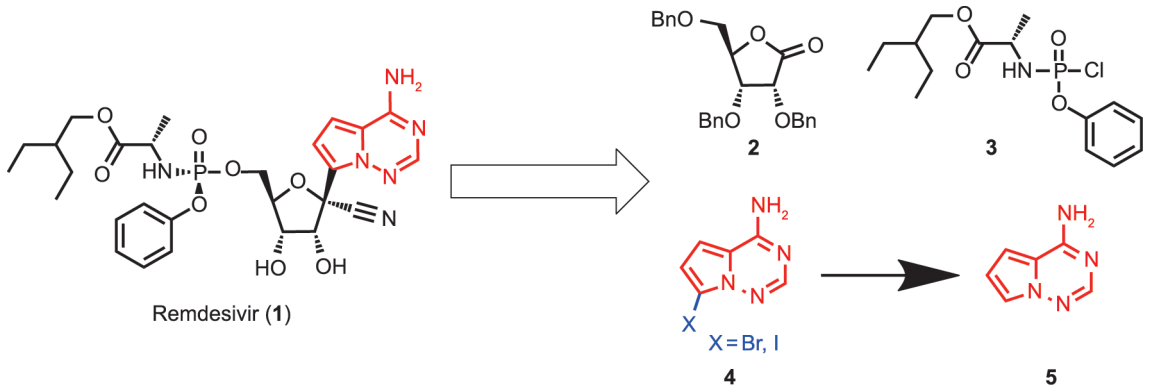

Fig. 1. General retrosynthetic analysis for remdesivir (**1**).

large quantity of the nucleobase unit **4** would be needed for the development of efficient methods to perform the key C-glycosylation step at a later stage, we first focused on the synthesis of the nucleobase unit **4** as part of our ongoing synthetic program directed toward the development of a next-generation synthetic protocol for the fast and scalable preparation of remdesivir.

Several synthetic routes to access the key intermediate pyrrolo-[2,1-*f*][1,2,4]triazin-4-amine (**5**) have been reported [12–16]. Simple bromination or iodization of **5** can lead to the target compound **4**. As a typical example, the synthesis of 7-bromopyrrolo[2,1-*f*]-[1,2,4]triazin-4-amine (**4** when X = Br) is described in this work. O'Connor et al. [12] and Dixon et al. [13] disclosed a route that was initiated by reacting 2,5-dimethoxytetrahydrofuran with *tert*-butyl carbazate to provide NH-*t*-butyloxycarbonyl (BOC) protected 1-amino-pyrrole. Subsequent cyanation with chlorosulfonyl isocyanate and *N*,*N*-dimethylformamide (DMF) led to NH-BOC-protected 1-amino-1*H*-pyrrole-2-carbonitrile. BOC deprotection, followed by cyclization with formamidine acetate (FAA) and potassium phosphate in ethanol at reflux, afforded the desired **5** [12,13]. Knapp et al. [14] reported a similar protocol in which 5-dimethoxytetrahydrofuran was transformed into 1-amino-pyrrole or NH-BOC-protected 1-amino-pyrrole by reacting with 2-aminoisoindole-1,3-dione or *tert*-butyl carbazate. Treatment of 1-amino-pyrrole with NaOAc in formic acid or treatment of NH-BOC-protected 1-amino-pyrrole with acetic anhydride in formic acid both led to *N*-(1*H*-pyrrol-1-yl)formamide. Condensation of *N*-(1*H*-pyrrol-1-yl)formamide with cyanamide afforded *N*′-cyano-*N*-(1*H*-pyrrol-1-yl)formimidamide; after cyclization mediated by a Lewis acid, **5** was obtained [14]. Patil et al. [15] reported a two-step route, in which pyrrole-2-carboxaldehyde was treated with hydroxylamine-*O*-sulfonic acid (HOSA) and KOH in water to produce 1-amino-1*H*-pyrrole-2-carbonitrile. Treatment of the chromatographed 1-amino-1*H*-pyrrole-2-carbonitrile with FAA in refluxing ethanol in the presence of potassium carbonate yielded **5** [15]. Unfortunately, the practical applications of these methods are hampered by the limited availability and relatively high cost of the non-commodity starting materials, as well as the requirement of flash column chromatography to isolate the relevant intermediates. Paymode et al. [16] recently published an approach that began with the formylation of pyrrole via a Vilsmeier–Haack reaction using phosphoryl chloride ($POCl_3$) and DMF. This was followed by the oxidative transformation of the resulting pyrrole-2-carboxaldehyde into pyrrole-2-carbonitrile by reacting it with hydroxylamine, acetic anhydride, and pyridine. Subsequent N-amination and cyclization afforded the desired **5**. Advantageously, this strategy proceeded from readily available and inexpensive commodity materials. However, the use of $POCl_3$ led to the generation of phosphorus-containing wastewater, which can have a profoundly detrimental effect on the environment. The use of hydroxylamine, acetic anhydride, and pyridine (3.5–5.0 equivalents (equiv.)) for the oxidative transformation not only increased the level of difficulty of product purification, but also increased the overall cost of preparing **5**. Moreover, direct N-amination with chloramine required complex chloramine extraction and concentration processes in order to increase throughput, which would lead to high consumption of extraction solvent and energy at scale.

Based on the previous studies, we improved the synthetic protocol to access the nucleobase unit **4** in a chromatography-free manner from the inexpensive and readily available pyrrole, as shown in Fig. 2. The improved approach started with the conversion of pyrrole (**6**) into pyrrole-2-carboxaldehyde (**7**) through a Vilsmeier–Haack reaction. Instead of using the traditional Vilsmeier–Haack reagents $POCl_3$/DMF, we employed bis(trichloromethyl) carbonate (BTC) and DMF to form the Vilsmeier salt. Thus, the generation of phosphorus-containing wastewater was avoided.

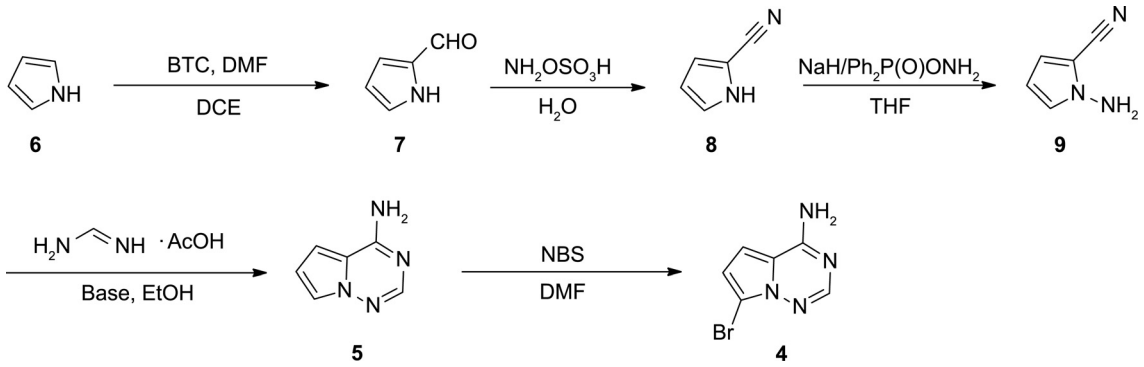

Fig. 2. Improved synthetic protocol to prepare 7-bromopyrrolo[2,1-*f*][1,2,4]triazin-4-amine (**4**). BTC: bis(trichloromethyl) carbonate; DCE: 1,2-dichloroethane; THF: tetrahydrofuran; NBS: *N*-bromosuccinimide.

Subsequently, treatment of pyrrole-2-carboxaldehyde (**7**) with the lower cost HOSA in water satisfactorily accomplished the oxidative transformation of the formyl functionality to obtain pyrrole-2-carbonitrile (**8**). This was followed by N-amination with *O*-(diphenylphosphinyl) hydroxylamine (DPPH) and cyclization with FAA to yield the key intermediate pyrrolo[2,1-*f*][1,2,4]triazin-4-amine (**5**). Finally, bromination with *N*-bromosuccinimide (NBS) led to the target compound, 7-bromopyrrolo[2,1-*f*][1,2,4]triazin-4-amine (**4**), with high regioselectivity and yield.

From a practical point of view, the traditional batch approach might suffer from a number of limitations, when it is scaled up. Firstly, the Vilsmeier–Haack and N-amination reactions are highly exothermic, and both involve extremely hazardous chemicals that cannot be easily controlled under batch conditions. Traditionally, these types of reactions have been performed in fed-batch mode, slowly dosing one of the reagents into the reaction mixture at a low temperature in order to prevent runaway scenarios due to insufficient mixing and slow heat dissipation in a batch reactor [17]. This is suitable for a small-scale batch process, but it does not appear to be amenable to large-scale production due to the excessively long addition time that might be needed as the surface-to-volume ratio is decreased. Hence, batch operation on a large scale can be time-consuming and inefficient. Moreover, ensuring a uniform temperature in the batch reactor is a major challenge due to the rapid reaction and insufficient mixing [18,19]. As a result, side reactions and further secondary reactions may be initiated, causing yield loss and safety problems. Secondly, the oxidative conversion of pyrrole-2-carboxaldehyde (**7**) to pyrrole-2-carbonitrile (**8**) is performed in an immiscible liquid–liquid biphasic mixture. The rate of mass transfer plays an important role in biphasic reactions, in which the overall reaction rate is affected by the rate of transfer of active species between the two phases. Thus, the oxidative transformation suffers from low mass transfer because only limited surface-to-volume ratios (up to ca. 2000 $m^2 \cdot m^{-3}$) are achievable in conventional batch reactors [20,21], which in turn results in limited apparent kinetics. Furthermore, the two-phase hydrodynamics in a batch reactor are a notoriously complex function of the reactor shape, size, impeller configuration, agitation speed, and so forth. This makes the scaling up of the reactor difficult and would postpone large-scale commercial production for years until the reaction kinetics and liquid–liquid hydrodynamics were well understood. Thirdly, the bromination reaction leading to the target compound **4** requires strict cryogenic conditions (from −20 to −78 °C) to ensure high selectivity. Maintaining cryogenic temperatures efficiently and consistently is difficult at scale for traditional batch reactors due to the fact that the volume increases much faster than the external surface area when upscaling a batch reactor to larger sizes [22]. Consequently, the low surface-to-volume ratios of batch reactors actually restrain the size of vessels for production. Last but not least, the batch processes are distinctly step-wise operations involving multistep reaction sequences, separations, and purifications [23]. Typically, after the completion of each synthetic reaction, the product is manually isolated from the reaction mixture and purified, and then the obtained pure product is employed in the next reaction. Such an approach is labor-intensive, resource-intensive, time-consuming, and often wasteful [23]. As a result, the production of a final API product (e.g., remdesivir) from raw materials can require up to 12 months, with large inventories of intermediates at several stages [9].

In recent years, there has been a growing trend in the pharmaceutical industry toward continuous manufacturing [24–26]. The uptake of microreactors has certainly played a central role in driving the transition from batch-based regimes to continuous-flow processing [27,28]. Compared with the traditional batch reactors, microreactors offer inherently small reaction volumes with fast mixing and excellent mass and heat transfer, which enables an improved reaction performance, a better safety profile, and more accurate control of reaction variables [29]. In addition, scaling up is generally considerably easier for a continuous process than for a batch process, as throughput can be increased either by numbering up the flow devices or by scaling up the reaction volumes [29]. Furthermore, multiple synthetic steps can be telescoped into a streamlined system by using flow processing, and laborious manual separation and the purification processes of intermediates can be avoided [30]. Therefore, significant resources, space, time, and energy can be saved by using state-of-the-art continuous-flow technology.

It was envisaged that the aforementioned limitations of the batch-wise synthesis could be overcome by employing continuous-flow technology. In this context, we aimed to develop an inherently safe, highly efficient, and scalable continuous-flow synthesis of the target compound **4**. In this approach, the reactions involving hazardous and unstable intermediates were facilitated, the exothermic reactions were well tamed, and the liquid–liquid biphasic reaction was significantly intensified. In addition, the cryogenic reaction was well accommodated. Furthermore, the workup procedures were fully integrated into the reaction sequences, forming a streamlined continuous-flow system that maximized the overall process efficiency.

2. Experimental section

2.1. Materials and reagents

The reagents and chemicals listed in Table 1 were employed without purification, unless otherwise indicated.

Where specified, 1,2-dichloroethane (DCE) and ethanol (EtOH) were dried by using molecular sieves (4 Å, 1 Å = 10^{-10} m). DMF and tetrahydrofuran (THF) were dried using the Vigor solvent purification system VSPS-7 (Vigor Gas Purification Technologies Co., Ltd., China).

2.2. General methods and analytics

Reactions were monitored by thin layer chromatography (TLC) on silica gel 60 F_{254} plates under ultraviolet (UV) light (254 nm). Flash chromatography was performed using silica gel 60 (230–400 mesh, Qingdao Haiyang Chemical Co., Ltd., China). Organic solutions were concentrated under reduced pressure on an IKA rotary evaporator (RE; RV10, Germany). Gas chromatography (GC)/mass spectrometry (MS) was performed on an Agilent 5977B GC (HP-5MS column, USA) with an Agilent 7830A MSD. GC analysis was performed on an Agilent 7890B (DB624 column) with a flame ionization detector. Melting points were measured on an MP450 digital melting point apparatus (Hanon Instruments, China). ^{1}H (400 MHz) and ^{13}C (100 MHz) nuclear magnetic resonance (NMR) was analyzed on a Bruker Avance 400 spectrometer (Germany) at ambient temperature. The chemical shifts are given in δ (ppm) units relative to tetramethylsilane (TMS). Coupling constant (J) values are given in hertz. Multiplicities are designated by the following abbreviations: s, singlet; d, doublet; t, triplet; q, quartet; br, broad; m, multiplet.

2.3. Experimental setup and method

Reactor I, Reactor II, Reactor IV, and Reactor V were constructed from perfluoroalkoxy (PFA) tubing with an inner diameter (ID) of 0.6 mm and outer diameter (OD) of 1.6 mm. Reactor III was a Coflore agitating cell reactor (ACR; AM Technology, UK), which features a Hastelloy reaction block mounted on a laterally shaking

Table 1
Reagent and chemical employed in this work.

Reagent and chemical	Abbreviation	Source	Purity
Ammonium chloride	NH_4Cl	RICHJOINT Chemical Reagents Co., Ltd. (Shanghai, China)	99.95%
Argon	Ar	Shanghai Tomoe Gases Co., Ltd. (Shanghai, China)	> 99.95%
Bis(trichloromethyl) carbonate	BTC	9DINGCHEM (Shanghai, China)	99%
Dichloromethane	DCM	Jiangsu Huai'an Chemical Technology (Huai'an, China)	≥ 99.5%
Ethyl acetate	EtOAc	Jiangsu Huai'an Chemical Technology (Huai'an, China)	≥ 99.5%
Ethanol	EtOH	Jiangsu Huai'an Chemical Technology (Huai'an, China)	≥ 99.9%
Formamidine acetate	FAA	Aladdin Biochemical Technology Co., Ltd. (Shanghai, China)	99%
Hydroxylamine-*O*-sulfonic acid	HOSA	Aladdin Biochemical Technology Co., Ltd. (Shanghai, China)	97%
Methanol	MeOH	Jiangsu Huai'an Chemical Technology (Huai'an, China)	> 99.9%
N,*N*-Dimethylformamide	DMF	Sinopharm Chemical Reagent Co., Ltd. (Shanghai, China)	99%
Nitrogen	N_2	Shanghai Tomoe Gases Co., Ltd. (Shanghai, China)	> 99.95%
N-Bromosuccinimide	NBS	BIDEPHARM (Shanghai, China)	98%
O-(Diphenylphosphinyl) hydroxylamine	DPPH	BIDEPHARM (Shanghai, China)	98%
Petroleum ether	PET	Jiangsu Huai'an Chemical Technology (Huai'an, China)	≥ 99.5%
Potassium *t*-butoxide	*t*-BuOK	BIDEPHARM (Shanghai, China)	98%
Potassium carbonate	K_2CO_3	RICHJOINT Chemical Reagents Co., Ltd. (Shanghai, China)	99.5%
Pyrrole	PYL	MACKLIN (Shanghai, China)	> 98%
Sodium chloride	NaCl	RICHJOINT Chemical Reagents Co., Ltd. (Shanghai, China)	99.5%
Sodium hydride	NaH	MACKLIN (Shanghai, China)	60%[a]
Sodium sulfate	Na_2SO_4	Shanghai Dahe Chemicals Co., Ltd. (Shanghai, China)	> 99.9%
Sodium sulfite	Na_2SO_3	Shanghai Dahe Chemicals Co., Ltd. (Shanghai, China)	> 99.9%
Tetrahydrofuran	THF	Rhawn Reagents (Shanghai, China)	99%
1,2-Dichloroethane	DCE	MACKLIN (Shanghai, China)	98%
1,8-Diazabicyclo[5.4.0]undec-7-ene	DBU	BIDEPHARM (Shanghai, China)	99.5%
1,3-Dibromo-5,5-dimethylhydantoin	DBDMH	BIDEPHARM (Shanghai, China)	98%

[a] Sodium hydride (NaH) was in the form of a 60% dispersion in mineral oil.

motor [31]. A central flow plate in the reaction block contains reaction chambers, interconnecting channels, and the agitators. The reaction chambers are made up of a series of individual cells of approximately 9.8 mL each with a freely moving agitator inside. The individual cells are joined by interconnecting channels that are 30 mm in length and 4 mm in width. The agitators move in rapidly reversing transverse movements in the cells when the reaction block is shaken by the shaking motor [32]. In principle, the reaction chambers emulate a cascade of milliliter-scale continuous stirred-tank reactors (CSTRs) for plug flow performance. For more details about the ACR, interested readers can refer to its user manual [31]. T-type micro-mixers were employed for mixing fluids in this work, unless otherwise indicated. It was found that good mixing was provided by using simple T-type micro-mixers for miscible fluids (steps 1, 4, and 5). However, when two streams were immiscible, the use of a T-type micro-mixer led to unideal mixing of the reacting streams. Therefore, a so-called two-phase cross-flow micro-mixer (CFMM) was employed to mix the immiscible liquids in step 2. In addition, several other types of equipment and devices, including a gas–liquid separator (GLS), continuous-flow solid filter (CFSF), miniature continuous stirred-tank reactor (m-CSTR), liquid–liquid membrane separator (LLMS), annular centrifugal extractor (ACE), and fixed-bed reactor (FBR), were used to integrate the workup procedures into the reaction sequences. A detailed description of the continuous-flow equipment and devices used in this work is provided in Section S3 in Appendix A.

Solutions were pumped using syringe pumps (Fusion 101, Fusion 200, Fusion 4000, Fusion 6000; Chemyx, USA) or high-performance liquid chromatography (HPLC) pumps (SF1005A, Sanotac, China). Slurries were pumped using peristaltic pumps (Model 77200-60, Masterflex, Germany). Back pressure regulators (BPRs) were purchased from Chemtrix (the Netherlands). Standard 1/4″-28 in-line check values (IDEX Health & Science, USA) were used to prevent reverse flow. Standard 1/4″-28 thread fittings with 1/16″ tubing and union connectors (Runzefluidsystem, China) were employed for fluid connections.

3. Results and discussion

Step 1 involved a Vilsmeier–Haack reaction of pyrrole (**6**) with DMF and BTC to form pyrrole-2-carboxaldehyde (**7**). Contact between DMF and BTC leads to fast formation of the Vilsmeier complex, which is thermally unstable and can generate high and fast temperature and pressure rises when heated [33,34]. This creates safety concerns, particularly when operated at scale [18,19]. In batch mode, this transformation was thus carried out by slowly dosing BTC solution into a mixture of pyrrole and DMF at 0 °C [17]. Upon completion of the addition, the reaction mixture was then heated to a higher temperature (45 °C) for further reaction. It took over 5 h to complete a millimole-scale reaction in batch mode (for a detailed description, see Section S2.1 in Appendix A). Our initial attempt to perform the reaction in flow without installing a GLS at the exit of Reactor I resulted in 95% conversion of **6** to **7** when two streams of reactants (1.0 equiv. PYL with 1.05 equiv. DMF in DCE, and 0.35 equiv. BTC in DCE) were mixed via a T-type micro-mixer with a theoretical residence time (i.e., the internal volume of Reactor I divided by the total flow rate) of 30 min (step 1 in Fig. 3). Nevertheless, it was observed that gas formed quickly in the flow reactor, leading to an unsteady flow rate of the reaction mixture and causing the actual residence time to be uncontrollable. To solve this problem, a GLS was connected after Reactor I, nitrogen (N_2) was fed into the GLS via its pressurized gas inlet, and an adjustable BPR was installed on its gas outlet. In this approach, the upstream Reactor I was stably pressurized by N_2 at a set pressure controlled by the BPR. The reaction mixture discharged from the GLS was then streamed into m-CSTR-1 (Fig. 3), along with an incoming saturated Na_2CO_3 aqueous solution to facilitate hydrolyzation of the intermediate immonium salt to obtain the formyl compound **7**.

Based on the improved flow system, further optimization (Table 2) led to the discovery that a lower temperature of 35 °C and 3 bar (1 bar = 10^5 Pa) back pressure resulted in a full conversion of **6** to **7** at a residence time of 5 min.

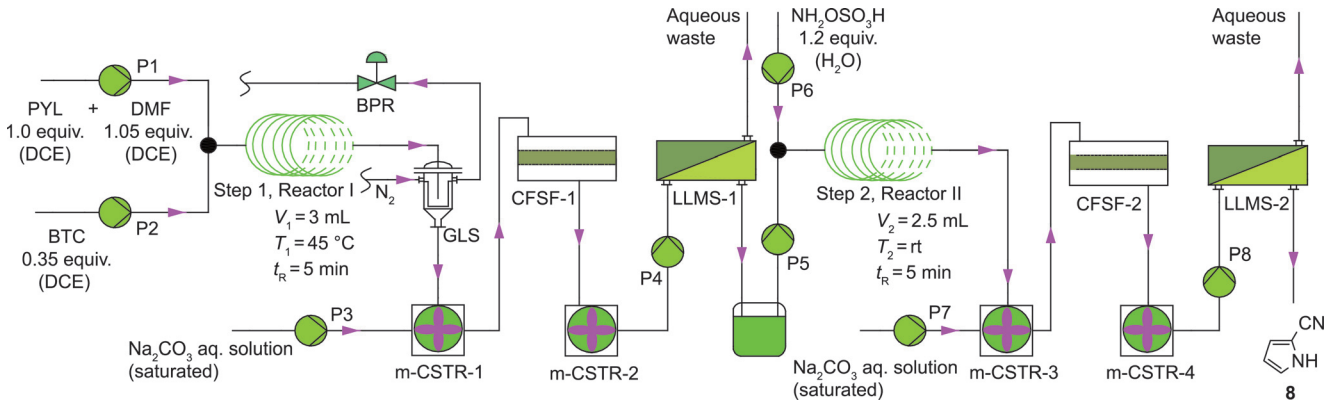

Fig. 3. Schematic representation of the two-step continuous-flow synthesis of pyrrole-2-carbonitrile (**8**). P1–P8 are pumps. *V*: internal volume of reactor; *T*: temperature of reactor; t_R: residence time; rt: room temperature. BTC: bis(trichloromethyl) carbonate; DCE: 1,2-dichloroethane; THF: tetrahydrofuran; NBS: *N*-bromosuccinimide. aq.: aqueous.

Table 2
Optimization of the continuous-flow synthesis of **7** in Reactor I.

Entry	F_{P1} (mL·min^{-1})	F_{P2} (mL·min^{-1})	t_R (min)[a]	*T* (°C)	*P* (bar)	Conversion[b]
1	0.11	0.19	10	45	2	100%
2	0.22	0.38	5	45	2	87%
3	0.11	0.19	10	45	3	100%
4	0.22	0.38	5	45	3	100%
5	0.22	0.38	5	45	4	100%
6	0.22	0.38	5	35	3	100%
7	0.22	0.38	5	30	3	96%
8	0.22	0.38	5	25	3	97%
9	0.22	0.38	5	18	3	97%

F_{P1}: flow rate of the P1 pump; F_{P2}: flow rate of the P2 pump; *P*: back pressure.
[a] Molar ratios were maintained when varying residence time.
[b] The conversion of **6** was determined by the GC/MS peak area percentage.

With a satisfactory flow approach to access **7**, we next sought to couple step 2 to step 1 in flow (Fig. 3). As solid salt was formed in m-CSTR-1, the collective flow stream was then pumped into CFSF-1 to remove the solids that clogged downstream Reactor II. In step 2, the oxidative conversion of pyrrole-2-carboxaldehyde (**7**) with HOSA yielded pyrrole-2-carbonitrile (**8**). In preliminary experiments, the filtrate from CFSF-1 and the HOSA (1.2 equiv.) aqueous solution were directly streamed into Reactor II via a two-phase CFMM. In this way, it was found that the optimal result was only a 79% conversion of **7** with a residence time of 30 min. This was an unsatisfactory outcome. The presence of an aqueous phase in the filtrate from CFSF-1 might have impaired the reactivity of **7** in the subsequent step 2. Hence, we later incorporated LLMS-1 after CFSF-1. The filtrate was delivered to LLMS-1 via m-CSTR-2 to get rid of the aqueous phase in a continuous manner. The organic phase outgoing from LLMS-1 was then mixed with the HOSA aqueous solution via a CFMM, and the resulting mixture was processed through Reactor II. This revised protocol proceeded with 100% conversion of **7** to **8** at room temperature with a residence time of 5 min, after a careful optimization (Table 3).

The output from Reactor II was then streamed into m-CSTR-3 together with an incoming saturated Na_2CO_3 aqueous solution. Because solid salt was formed in m-CSTR-3, the mixture was then passed through CFSF-2 to remove the solids that would block LLMS-2. The installation of LLMS-2 allowed fast separation of the organic phase from the biphasic mixture. The optimized two-step reaction-workup integrated-flow process yielded **8** in an isolated yield of 47.6% with a throughput of 3.02 g·h^{-1}.

Step 3 involved the N-amination of pyrrole-2-carbonitrile (**8**) to obtain 1-amino-1*H*-pyrrole-2-carbonitrile (**9**). The involvement of NaH in this reaction would pose potential safety hazards, especially on a large scale. Therefore, the batch reaction was implemented by means of slowly dosing the substrate **8** in dry THF into the NaH–THF mixture, followed by the dropwise addition of $Ph_2P(O)ONH_2$ in THF (for a detailed description, see Section S2.3 in Appendix A). As such, the batch operation suffered from low levels of efficiency and productivity. Initial efforts to translate this reaction into a microchannel-based flow process were hindered by the fact that NaH and $Ph_2P(O)ONH_2$ are insoluble in THF and because solid byproducts were produced. To address this issue, we employed a Coflore ACR to facilitate the flow processing of slurries. Given the complexity of directly coupling the ACR into the previous two-step flow sequence, we first examined the independent flow processing using purified pyrrole-2-carbonitrile (**8**) (Fig. 4). The two streams of reactants (1.0 equiv. **8** with 1.2 equiv. $Ph_2P(O)ONH_2$ in THF, and 1.40–3.47 equiv. NaH in THF) were fed into the ACR at accurately controlled flow rates. It was found that the stoichiometry and residence time exerted substantial influences on the reaction in flow, so their effects were examined (Table 4).

The results revealed that a molar ratio of NaH to $Ph_2P(O)ONH_2$ of less than 1.87 led to a maximum 50% conversion of **8**, albeit at a relatively longer residence time of 16 min. Furthermore, a higher molar ratio of 2.175 (NaH:$Ph_2P(O)ONH_2$) resulted in a full conversion of **8** within only 6 min, when one equivalent of substrate **8** was used. Under the optimal flow conditions of 30 °C with a residence time of 6 min, we gratifyingly obtained a 97% isolated yield of **9**. It is worth noting that the reaction time was only 6 min in flow, while the batch process required over 5 h (for a detailed description, see Section S2.3 in Appendix A). Moreover, continuous processing was easily maintained through the ACR for a period of over 10 h. Hence, it was demonstrated that the continuous-flow processing of slurries could be successfully performed using the ACR.

Table 3
Optimization of the continuous-flow synthesis of 8 in Reactor II.

Entry	F_{P5} (mL·min^{-1})	F_{P6} (mL·min^{-1})	t_R (min)[a]	T	Conversion[b]
1	0.101	0.024	20	rt	100%
2	0.203	0.047	10	rt	100%
3	0.253	0.059	8	rt	100%
4	0.406	0.094	5	rt	100%

F_{P5}: flow rate of the P5 pump; F_{P6}: flow rate of the P6 pump.
[a] Molar ratios were maintained when varying residence time.
[b] The conversion of **7** was determined by the GC/MS peak area percentage.

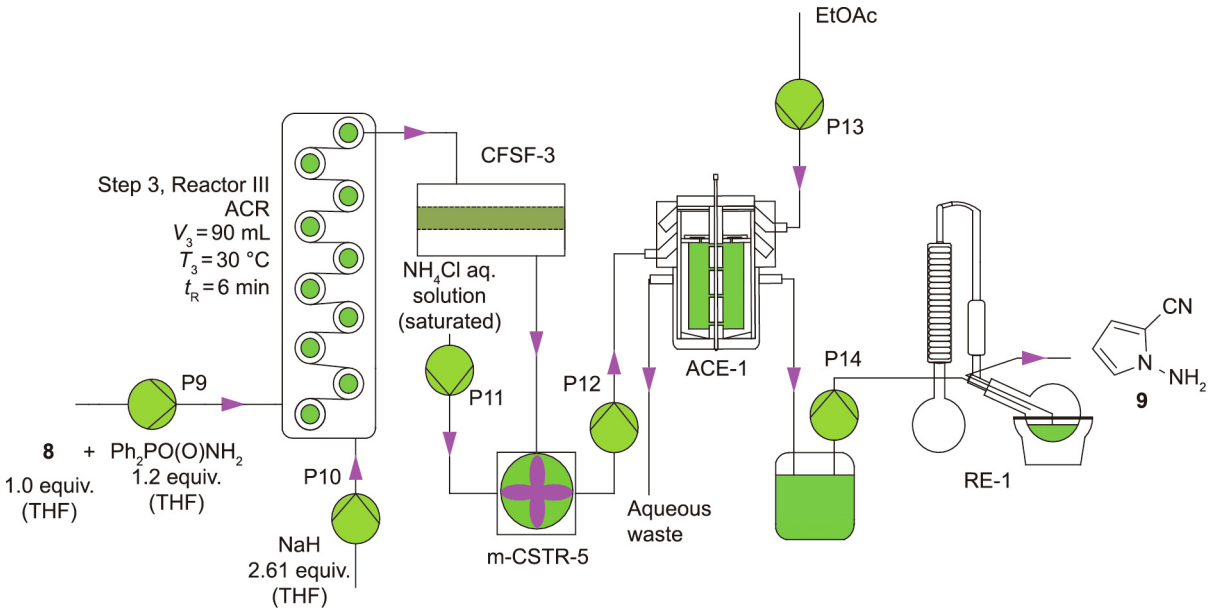

Fig. 4. 1-Amino-1*H*-pyrrole-2-carbonitrile (**9**) formation in flow. P9–P14 are pumps. aq: aqueous.

Table 4
Optimization of the continuous-flow synthesis of **9** in Reactor III.

Entry	F_{P9} (mL·min^{-1})	F_{P10} (mL·min^{-1})	Molar ratio of **8**:DPPH:NaH	t_R (min)[a]	T (°C)	Conversion[b]
1	2.843	2.879	1.0:1.2:2.24	10	30	45%
2	3.781	2.401	1.0:1.2:1.40	11	30	40%
3	3.781	2.401	1.0:1.2:1.40	16	30	44%
4	2.843	2.879	1.0:1.2:2.24	12	30	50%
5	2.843	3.357	1.0:1.2:2.61	6	30	100%
6	2.843	3.357	1.0:1.2:2.61	10	30	100%
7	2.139	3.357	1.0:1.2:3.47	6	30	100%
8	2.139	3.357	1.0:1.2:3.47	10	30	100%

F_{P9}: flow rate of the P9 pump; F_{P10}: flow rate of the P10 pump.
[a] Because the formed gas affected the actual total flow rate, this was the measured actual residence time.
[b] The conversion of **8** was determined by the GC peak area percentage.

Subsequently, we examined the synthesis of **9** from **6** in a three-step fully continuous flow process. Since the effluent from Reactor II was an immiscible liquid–liquid mixture of DCE and the aqueous phase, the existence of water would undoubtedly deactivate NaH and hence impede the reaction of step 3. Therefore, CFSF-2 and LLMS-2 were coupled sequentially to Reactor II (Fig. 5). The output from Reactor II was continuously filtrated; then, the filtrate was streamed into LLMS-2 to separate out the organic phase. Following the optimized flow protocol of step 3, the organic phase output from LLMS-2 was streamed into the ACR along with the incoming $Ph_2P(O)ONH_2$ (1.2 equiv.) in THF and NaH (2.61 equiv.) in THF to enable the three-step fully continuous flow synthesis of **9**. The outgoing suspension from the ACR was then immediately filtered via CFSF-3; meanwhile, the filtrate was streamed into m-CSTR-5 along with the incoming saturated NH_4Cl aqueous solution. The collective mixture was then pumped through ACE-1 together with EtOAc in order to continuously extract the product **9** into the organic phase. The organic phase output from ACE-1 was subsequently pumped into RE-1, working under reduced pressure, to quickly remove the solvent. The three-step continuous synthesis achieved a 44.3% isolated yield of **9** in a total residence time of 34 min with a throughput of 2.6 g·h^{-1}.

In step 4, 1-amino-1*H*-pyrrole-2-carbonitrile (**9**) was cyclized with FAA promoted by a base to obtain pyrrolo[2,1-*f*][1,2,4]-triazin-4-amine (**5**). The initial batch cyclization reaction was performed through a combination of purified **9** in ethanol with FAA and K_2CO_3 at 85 °C. The batch reaction required 10 h to reach complete conversion (for a detailed description, see Section S2.4 in

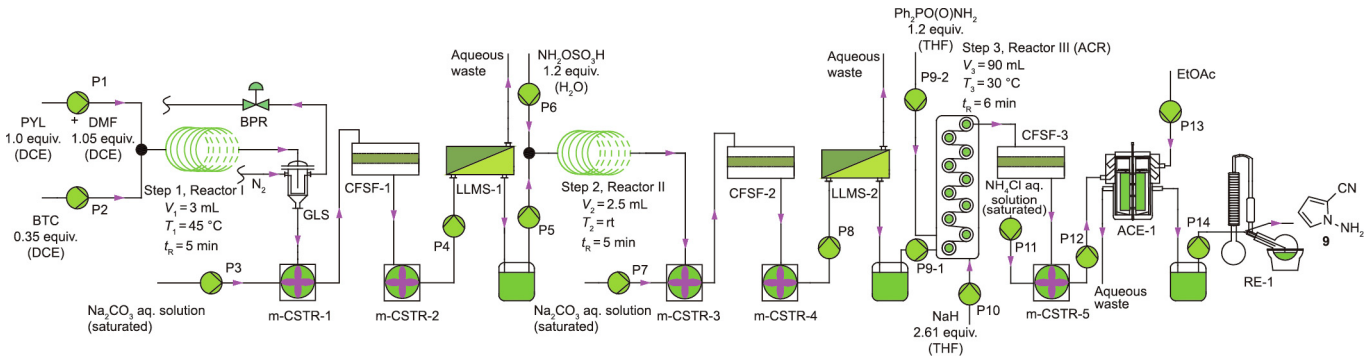

Fig. 5. Schematic representation of the three-step continuous-flow synthesis of 1-amino-1*H*-pyrrole-2-carbonitrile (**9**).

Appendix A). Since K_2CO_3 existed as a solid in ethanol, we attempted to load K_2CO_3 into a FBR, and then pump **9** and FAA solution through it in order to translate the batch process to flow. Unfortunately, it turned out that no reaction was detected in this mode under any conditions. We then attempted to use 1,8-diazabicyclo[5.4.0]undec-7-ene (DBU) as the base instead, as it is fully soluble in ethanol. Its batch operation achieved full conversion in 4 h—much faster than K_2CO_3-mediated cyclization (for a detailed description, see Section S2.4 in Appendix A). Based on the batch protocol, the DBU-mediated cyclization was first independently examined in flow. A solution of **9** (1.0 equiv.), FAA (12 equiv.), and DBU (13 equiv.) in EtOH was allowed to pass through Reactor IV, which was pressurized by a BPR to avoid boiling point limitations (Fig. 6). Initially, poor conversion (< 10%) was resulted from operating the flow reaction at 85 °C and 5 bar back pressure with a residence time of 20 min. When we increased the reaction temperature to 120 °C, the conversion rose to 75%. A further increase in reaction temperature required a simultaneous increase in the back pressure in order to maintain ethanol as a liquid. Further optimization led to a good conversion at 140 °C and 10 bar back pressure with 30 min of residence time (Table 5). As such, the ability of flow processing to operate at high temperatures in a low-boiling solvent was well exploited.

With a workable flow protocol to access **5**, we next directed our focus to the preparation of pyrrolo[2,1-*f*][1,2,4]triazin-4-amine (**5**) from the starting material **6** via a four-step process by integrating reactions with separation units in a further endeavor to work toward our goal of fully continuous synthesis. The output from RE-1 was streamed to a T-type micro-mixer along with a solution of FAA (12 equiv.) and DBU (13 equiv.) in EtOH, and the resultant mixture was processed through Reactor IV (Fig. 7). The outcome from Reactor IV was streamed into m-CSTR-6 along with the incoming saturated NH_4Cl aqueous solution (Fig. 7). The combined outcome was then pumped through ACE-2 together with EtOAc in order to continuously extract the product **5** into the organic phase. The organic phase output from ACE-2 was subsequently pumped into RE-2, working under reduced pressure, to quickly remove the solvent (Fig. 7). Under the optimal four-step sequential flow operations with a total residence time of 74 min, we obtained 27.7% isolated yield of **5**.

The last reaction (step 5) was the bromination of pyrrolo[2,1-*f*]-[1,2,4]triazin-4-amine (**5**) to produce the target compound 7-bromopyrrolo[2,1-*f*][1,2,4]triazin-4-amine (**4**). In our early-stage attempts, we carried out the bromination reaction in batch using 1,3-dibromo-5,5-dimethylhydantoin (DBDMH) as the brominating agent (for a detailed description, see Section S2.5 in Appendix A). The results were poor in terms of conversion and selectivity (Table S1 in Appendix A). Either over-bromination occurred when the substrate was fully converted, or only modest conversions (68%–64%) of the substrate were achieved with relatively low regioselectivities (63%–84%) for the target compound **4**. We then experimented with NBS as the brominating agent. In batch, it was revealed that good conversion and regioselectivity were obtained when brominating with NBS at −40 °C, while the conversion declined to 81% when the reaction temperature was decreased to −78 °C (Table S2 in Appendix A). Having achieved the reaction conditions to obtain **4**, we then examined the bromination step in flow as a discrete operation using purified **5**. The batch

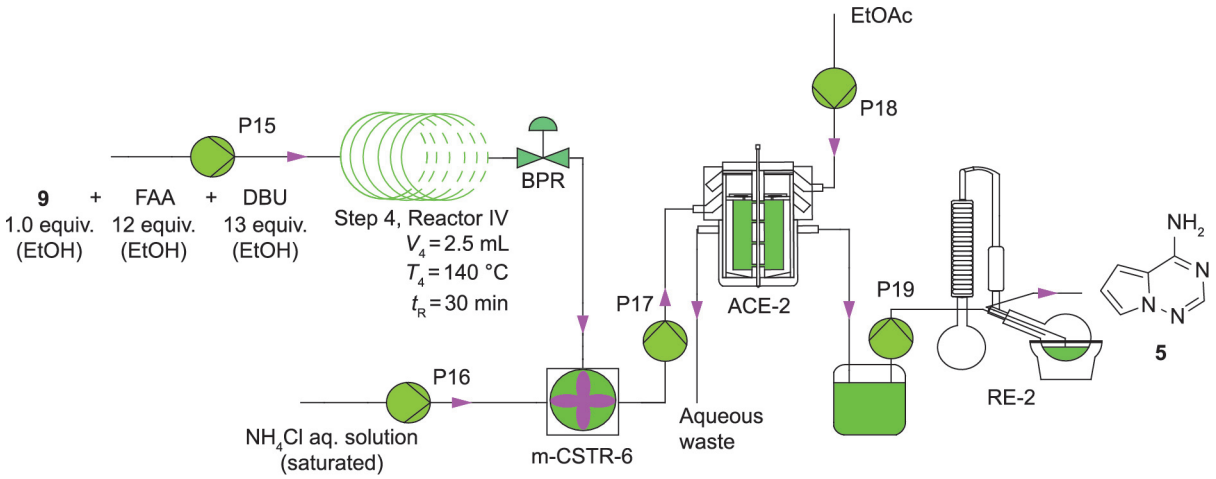

Fig. 6. Pyrrolo[2,1-*f*][1,2,4]triazin-4-amine (**5**) formation in flow. P15–P19 are pumps.

Table 5
Optimization of the continuous-flow synthesis of **5** in Reactor IV.

Entry	F_{P15} (mL·min^{-1})	t_R (min)	T (°C)	P (bar)	Conversion[a]
1	0.130	20	85	5	< 10%
2	0.130	20	120	5	75%
3	0.130	20	140	10	90%
4	0.083	30	140	10	> 95%

F_{P15}: flow rate of the P15 pump.
[a] Conversion was determined by the GC/MS peak area percentage.

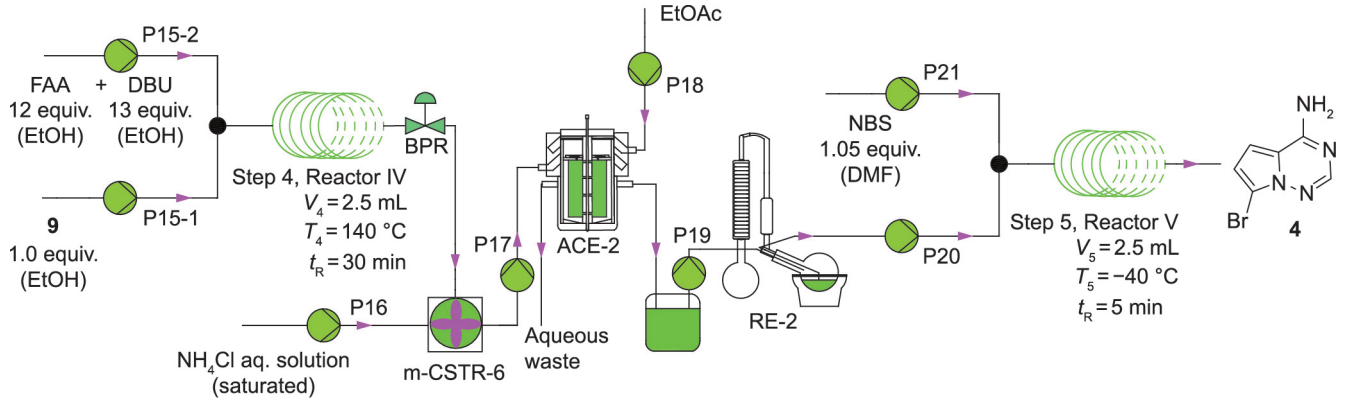

Fig. 7. Schematic representation of the continuous-flow synthesis of **4**. P20 and P21 are pumps.

Table 6
Optimization of the continuous-flow synthesis of **4** in Reactor V.

Entry	F_{P20} (mL·min^{-1})	F_{P21} (mL·min^{-1})	t_R (min)	Conversion[a]	Selectivity[b]		
					7-Bromopyrrolo[2,1-*f*]-[1,2,4]triazin-4-amine	5-Bromopyrrolo[2,1-*f*]-[1,2,4]triazin-4-amine	5,7-Dibromopyrrolo[2,1-*f*]-[1,2,4]triazin-4-amine
1	0.25	0.25	5	100%	83%	10%	5%
2	0.42	0.41	3	94%	85%	11%	3%
3	1.26	1.23	1	91%	86%	11%	2%

F_{P20}: flow rate of the P20 pump; F_{P21}: flow rate of the P21 pump.
[a] Conversion was determined by the GC/MS peak area percentage.
[b] Selectivity was determined by the GC/MS peak area percentage.

conditions translated well to flow, with full conversion of **5** being observed at −40 °C with a residence time of 5 min (Table 6).

Finally, we examined the synthesis of **4** from **6** in a five-step fully continuous-flow process. In connecting step 5 to the established previous four steps, the output from RE-2 was streamed to a T-type micro-mixer along with a solution of NBS (1.05 equiv.) in DMF, and the combined mixture was then streamed through Reactor V. The outcome from Reactor V was collected and purified offline. Overall, the five-step flow process produced 7-bromopyrrolo[2,1-*f*][1,2,4]triazin-4-amine (**4**) with an isolated yield of 14.1%, in a total residence time of 79 min with a throughput of 2.96 g·h^{-1}.

The striking advantages of the continuous-flow approach are twofold. First, the reaction times in flow were considerably reduced compared with those of the conventional batch approach (Table 7). The total reaction time of the batch approach was more than 19 h, while that of the continuous-flow approach was only 51 min. Since time-consuming workup procedures were involved in the batch procedures, the total time (i.e., reaction time plus post-reaction workup time) consumed in the batch-wise synthesis was more than 26.5 h (the corresponding workup procedures took at least 7.5 h in total). In contrast, the total residence time in the continuous processing was only 79 min, thus affording a time-efficient synthesis of the target compound 7-bromopyrrolo[2,1-*f*]-[1,2,4]triazin-4-amine (**4**). Second, the safety profile under continuous-flow conditions was significantly enhanced compared with that in the batch approach.

Table 7
Comparison between the conventional batch approach and the continuous-flow approach.

Reaction steps	Reaction time[a]	
	Conventional batch approach (h)	Continuous-flow approach (min)
Step 1	5.50–5.75	5
Step 2	1.00	5
Step 3	5.75	6
Step 4	4.00	30
Step 5	2.75	5
Steps 1–5	> 19.00	51

[a] The post-reaction workup time was not included.

4. Conclusions

In summary, we have developed a five-step fully continuous-flow synthesis of 7-bromopyrrolo[2,1-*f*][1,2,4]triazin-4-amine (**4**), which is the nucleobase unit of the antiviral drug remdesivir, based

on an improved protocol from the widely available and inexpensive starting material pyrrole. Under the optimal flow conditions, we obtained 14.1% isolated yield of the target compound **4** in a total residence time of 79 min with a throughput of 2.96 $g \cdot h^{-1}$. The total residence time in the continuous processing was significantly shorter than the total time consumed in the batch approach (> 26.5 h). The exothermic reactions involving hazardous and unstable intermediates, liquid–liquid biphasic oxidative transformation, and a cryogenic reaction were facilitated in flow. Notably, the workup procedures, including solid filtration, liquid–liquid separation, liquid–liquid extraction, and reduced-pressure evaporation, were continuously addressed by deploying dedicated equipment and devices that were fully integrated into the reaction sequences. The integration of the workup procedures and multiple chemical transformations into a single streamlined continuous-flow system made it possible to circumvent laborious and time-consuming separation and purification processes of intermediates, and thus enabled a rapid manufacturing time with minimal resources and energy consumption, as well as minimal waste generation. This work represents a step forward toward the development of a next-generation synthetic protocol for the fast and scalable preparation of remdesivir.

Acknowledgments

This work was supported by the Chinese Academy of Engineering (2020-KYGG-01-01) and the National Natural Science Foundation of China (21908029).

Compliance with ethics guidelines

Yongxing Guo, Minjie Liu, Meifen Jiang, Yuan Tao, Dang Cheng, and Fen-Er Chen declare that they have no conflict of interest or financial conflicts to disclose.

Appendix A. Supplementary data

Supplementary data to this article can be found online at https://doi.org/10.1016/j.eng.2021.07.029.

References

[1] Lamb YN. Remdesivir: first approval. Drugs 2020;80(13):1355–63.
[2] US Food and Drug Administration. FDA approves first treatment for COVID-19 [Internet]. Silver Spring: US Food and Drug Administration; 2020 Oct 22 [cited 2021 Feb 18]. Available from: https://www.fda.gov/news-events/press-announcements/fda-approves-first-treatment-covid-19.
[3] Views of COVID-19 studies listed on ClinicalTrials.gov (Beta) [Internet]. Bethesda: US National Library of Medicine; [cited 2021 Jun 18]. Available from: https://clinicaltrials.gov/ct2/covid_view.
[4] World Health Organization. WHO recommends against the use of remdesivir in COVID-19 patients [Internet]. Geneva: World Health Organization; 2020 Nov 20 [cited 2021 Feb 18]. Available from: https://www.who.int/news-room/feature-stories/detail/who-recommends-against-the-use-of-remdesivir-in-covid-19-patients.
[5] World Health Organization. WHO coronavirus (COVID-19) dashboard [Internet]. Geneva: World Health Organization; [cited 2021 Jun 18]. Available from: https://covid19.who.int.
[6] National Center for Immunization and Respiratory Diseases (NCIRD), Division of Viral Diseases. What you need to know about variants [Internet]. Atlanta: US Department of Health & Human Services; [cited 2021 Jun 18]. Available from: https://www.cdc.gov/coronavirus/2019-ncov/transmission/variant.html.
[7] International SOS. COVID-19 variants [Internet]. London: International SOS; [cited 2021 Jun 18]. Available from: https://pandemic.internationalsos.com/2019-ncov/covid-19-variants.
[8] Jarvis LM. Scaling up remdesivir amid the coronavirus crisis [Internet]. Washington, DC: American Chemical Society; 2020 Apr 20 [cited 2021 Feb 18]. Available from: https://cen.acs.org/biological-chemistry/infectious-disease/Scaling-remdesivir-amid-coronavirus-crisis/98/web/2020/04.
[9] Gilead Sciences, Incorporation. Working to supply Veklury® for COVID-19 [Internet]. Foster: Gilead Sciences, Incorporation; 2020 Oct 22 [cited 2021 Feb 18]. Available from: https://www.gilead.com/purpose/advancing-global-health/covid-19/working-to-supply-veklury-for-covid-19.
[10] Siegel D, Hui HC, Doerffler E, Clarke MO, Chun K, Zhang L, et al. Discovery and synthesis of a phosphoramidate prodrug of a pyrrolo[2,1-*f*][triazin-4-amino]-adenine C-nucleoside (GS-5734) for the treatment of Ebola and emerging viruses. J Med Chem 2017;60(5):1648–61.
[11] Warren TK, Jordan R, Lo MK, Ray AS, Mackman RL, Soloveva V, et al. Therapeutic efficacy of the small molecule GS-5734 against Ebola virus in rhesus monkeys. Nature 2016;531(7594):381–5.
[12] O'Connor S, Dumas J, Lee W, Dixon J, Cantin D, Gunn D, et al. Pyrrolo[2,1-*f*]-[1,2,4]triazin-4-ylamines IGF-1R kinase inhibitors for the treatment of cancer and other hyperproliferative diseases. United States Patent 8431695. 2013 Apr 30.
[13] Dixon JA, Phillips B, Achebe F, Kluender HCE, Newcom J, Parcella K, et al. Substituted 4-amino-pyrrolotriazine derivatives useful for treating hyperproliferative disorders and diseases associated with angiogenesis. United States Patent 8143393. 2007 Jul 6.
[14] Knapp RR, Tona V, Okada T, Sarpong R, Garg NK. Cyanoamidine cyclization approach to remdesivir's nucleobase. Org Lett 2020;22(21):8430–5.
[15] Patil SA, Otter BA, Klein RS. Synthesis of pyrrolo[2,1-*f*][1,2,4]triazine congeners of nucleic acid purines via the N-amination of 2-substituted pyrroles. J Heterocycl Chem 1994;31(4):781–6.
[16] Paymode DJ, Cardoso FSP, Agrawal T, Tomlin JW, Cook DW, Burns JM, et al. Expanding access to remdesivir via an improved pyrrolotriazine synthesis: supply centered synthesis. Org Lett 2020;22(19):7656–61.
[17] Shan WG, Shi XJ, Su WK. Vilsmeier–Haack synthesis of aromatic aldehydes using bis-(trichloromethyl) carbonate and dimethylformamide. Org Prep Proced Int 2004;36(4):337–40.
[18] Huzmezan M, Gough B, Kovac S. Advanced control of batch reactor temperature. In: Proceedings of the 2002 American Control Conference; 2002 May 8–10; Anchorage, AK, USA; 2002. p. 1156–61.
[19] Caccavale F, Iamarino M, Pierri F, Tufano V. Control and monitoring of chemical batch reactors. London: Springer; 2011.
[20] Jovanović J, Rebrov EV, Nijhuis TA, Hessel V, Schouten JC. Phase-transfer catalysis in segmented flow in a microchannel: fluidic control of selectivity and productivity. Ind Eng Chem Res 2010;49(6):2681–7.
[21] Gemoets HPL, Su Y, Shang M, Hessel V, Luque R, Noël T. Liquid phase oxidation chemistry in continuous-flow microreactors. Chem Soc Rev 2016;45(1):83–117.
[22] Worstell J. Batch and semi-batch reactors—practical guides in chemical engineering. Oxford: Butterworth-Heinemann; 2015. p. 51–84.
[23] Webb D, Jamison TF. Continuous flow multi-step organic synthesis. Chem Sci 2010;1(6):675–80.
[24] Cole KP, Groh JM, Johnson MD, Burcham CL, Campbell BM, Diseroad WD, et al. Kilogram-scale prexasertib monolactate monohydrate synthesis under continuous-flow CGMP conditions. Science 2017;356(6343):1144–50.
[25] Adamo A, Beingessner RL, Behnam M, Chen J, Jamison TF, Jensen KF, et al. On-demand continuous-flow production of pharmaceuticals in a compact, reconfigurable system. Science 2016;352(6281):61–7.
[26] Liu C, Xie J, Wu W, Wang M, Chen W, Idres SB, et al. Automated synthesis of prexasertib and derivatives enabled by continuous-flow solid-phase synthesis. Nat Chem 2021;13(5):451–7.
[27] Liao J, Zhang S, Wang Z, Song X, Zhang D, Kumar R, et al. Transition-metal catalyzed asymmetric reactions under continuous flow from 2015 to early 2020. Green Synth Catal 2020;1(2):121–33.
[28] Calabrese GS, Pissavini S. From batch to continuous flow processing in chemicals manufacturing. AIChE J 2011;57(4):828–34.
[29] Gutmann B, Cantillo D, Kappe CO. Continuous-flow technology—a tool for the safe manufacturing of active pharmaceutical ingredients. Angew Chem Int Ed Engl 2015;54(23):6688–728.
[30] Fitzpatrick DE, Ley SV. Engineering chemistry: integrating batch and flow reactions on a single, automated reactor platform. React Chem Eng 2016;1(6):629–35.
[31] Coflore ACR laboratory scale flow reactor [Internet]. Cheshire: AM Technology; [cited 2021 Feb 18]. Available from: https://www.amt.uk/coflore-acr.
[32] Browne DL, Deadman BJ, Ashe R, Baxendale IR, Ley SV. Continuous flow processing of slurries: evaluation of an agitated cell reactor. Org Process Res Dev 2011;15(3):693–7.
[33] Bollyn M. Thermal hazards of the Vilsmeier–Haack reaction on *N,N*-dimethylaniline. Org Process Res Dev 2005;9(6):982–96.
[34] Miyake A, Suzuki M, Sumino M, Iizuka Y, Ogawa T. Thermal hazard evaluation of Vilsmeier reaction with DMF and MFA. Org Process Res Dev 2002;6(6):922–5.